Room-Temperature Preparation of ZrO_2 Precursor Thin Film in an Aqueous Peroxozirconium-Complex Solution

Yanfeng Gao, Yoshitake Masuda, Hiromichi Ohta, and Kunihito Koumoto*

Department of Applied Chemistry, Graduate School of Engineering, Nagoya University, Furo-cho, Chikusa-ku, Nagoya 464-8603, Japan

Received February 13, 2004. Revised Manuscript Received April 20, 2004

We report a deposition method for room-temperature preparation of ZrO_2 thin film using an aqueous solution. $ZrO(NO_3)_2 \cdot 2H_2O$ was dissolved in a solvent mixture composed of H_2O_2 and ammonia. The dissolving reaction produced a colorless, transparent peroxozirconium-complex solution which was unstable; decomposition occurred even at room temperature. Amorphous, transparent, dense ZrO_2 precursor thin films of up to 500 nm thick were prepared on a cleaned P-type Si substrate. The film showed good adhesion to the substrate as peel-off was not found after either sonication or a Scotch-tape peel-off test. The as-deposited thin film was of high purity with a composition of $ZrO_{1.4}(OH)_{1.2}$. No peroxo groups were present in the as-deposited film. Annealing caused crystallization of the amorphous film into tetragonal ZrO_2 at 500 °C and phase transformation from tetragonal to monoclinic ZrO_2 at higher temperatures. Both films showed very flat surfaces consisting of nanoparticles with homogeneous size of tens of nanometers in diameter. The optical band gap of the amorphous film was 5.0–5.75 eV, whereas it was 5.65 eV for the crystalline ZrO_2 thin film.

Introduction

Zirconia thin films are of importance due to their thermal, mechanical, and chemical stability,[1–4] and have attracted much attention for applications such as optical coatings,[5] buffer layers for growing superconductors,[6] thermal-shield or corrosion-resistant coatings,[7] ionic conductors,[8] and oxygen sensors.[9]

Two kinds of techniques, the self-assembled monolayer (SAM) technique[10–14] and the liquid-phase deposition (LPD) method,[15–17] have been developed for direct deposition of ZrO_2 thin films using aqueous solutions. Agarwal et al.[10] studied the deposition of ZrO_2 thin film on a SAM surface by enhanced hydrolysis of zirconium sulfate ($Zr(SO_4)_2 \cdot 4H_2O$) aqueous solution in the presence of HCl (pH <1) at 70 °C and confirmed the existence of two phases in the films produced from suspensions: nanocrystalline tetragonal (t)-ZrO_2 and amorphous basic zirconium sulfate. Niesen et al.[12] deposited ZrO_2 film from an aqueous solution at 70–80 °C onto a functionalized SAM-adsorbed silicon and suggested that an unstable precipitation reaction medium is required for film growth exceeding 3 nm in thickness. Polli et al.[14] produced nanocrystalline zirconia via SAM-mediated deposition from an aqueous dispersion without visible bulk precipitation. Note the same solution system as reported[10] was used in all these studies. Compared to SAM-grafted substrate, no continuous, adherent deposits were precipitated on a bare substrate (without SAM layer).[10] We have also prepared ZrO_2 thin film on a SAM surface by the controlled hydrolysis of $ZrOCl_2 \cdot 8H_2O$ in ethanol at 50 °C, and site-selective deposition was also developed.[11] However, a large amount of chlorine was present in the as-deposited thin film because of uncompleted hydrolysis reaction of zirconium ethoxide.

In the LPD process,[15–17] a soluble hexafluorozirconate salt (M_2ZrF_6, M = Na, K, NH_4, etc.) was employed as the zirconium species. These zirconium–fluoro-complex ions can hydrolyze in aqueous media by the release of fluorine ions, which can be further consumed by the reaction with boric acid or metal Al. Hence, the hydrolysis reactions proceed and deposit ZrO_2-based solid phase. The advantages of the LPD process are its mild

* To whom correspondence should be addressed. E-mail: g44233a@nucc.cc.nagoya-u.ac.jp. Fax: +81-52-789-3201. Tel: +81-52-789-3327.

(1) Shane, M.; Mecartney, M. L. *J. Mater. Sci.* **1990**, *25*, 1537–1544.
(2) Atik, M.; Zarzycki, J.; R' Kha, C. *J. Mater. Sci. Lett.* **1994**, *13*, 266–269.
(3) Di Maggio, R.; Fedrizzi, L.; Rossi, S.; Scardi, P. *Thin Solid Films* **1996**, *286*, 127–135.
(4) Quinson, J. F.; Chino, C.; Becdelievre, A. M.; Guizard, C.; Brunel, M. *J. Mater. Sci.* **1996**, *31*, 5179–5184.
(5) Wendel, H.; Holzschuh, H.; Suhr, H.; Erker, G.; Dehnicke, S.; Mena, M. *Mod. Phys. Lett. B* **1990**, *4*, 1215–1217.
(6) Komatsu, Y.; Sato, T.; Ito, S.; Akashi, K. *Thin Solid Films* **1999**, *341*, 132–135.
(7) Izumi, K.; Murakami, M.; Deguchi, T.; Morita, A. *J. Am. Ceram. Soc.* **1989**, *72*, 1465–1468.
(8) Cao, G.-Z.; Brinkman, H. W.; Meijerink, J.; De Vries, K. J.; Burggraaf, A. J. *J. Am. Ceram. Soc.* **1993**, *76*, 2201–2208.
(9) Bastianini, A.; Battiston, G. A.; Gerbasi, R.; Porchia, M.; Daolio, S. *J. Phys. IV* **1995**, *5*, 525–532.
(10) Agarwal, M.; De Guire, M. R.; Heuer, A. H. *J. Am. Ceram. Soc.* **1997**, *80*, 2967.
(11) Gao, Y.-F.; Masuda, Y.; Yonezawa, T.; Koumoto, K. *J. Ceram. Soc. Jpn.* **2002**, *110*, 379.
(12) Niesen, T. P.; De Guire, M. R.; Bill, J.; Aldinger, F.; Rühle, M.; Fischer, A.; Jentoft, F.; Schlögl, R. *J. Mater. Res.* **1999**, *14*, 2464–2475.
(13) Shin, H.; Agarwal, M.; De Guire, M. R. *Acta Mater.* **1998**, *46*, 801.
(14) Poli, A. D.; Wagner, T.; Fischer, A.; Weinberg, G.; Jentoft, F. C.; Schlögl, R.; Rühle, M. *Thin Solid Films* **2000**, *379*, 122–127.
(15) Yao, T.; Inui, T.; Ariyoshi, A. *J. Am. Ceram. Soc.* **1996**, *79*, 3329.
(16) Yao, T. *J. Mater. Res.* **1998**, *13*, 1091.
(17) Ozawa, N.; Yao, T. *Trans. Mater. Res. Soc. Jpn.* **2003**, *28*, 321.

10.1021/cm049771i CCC: $27.50 © 2004 American Chemical Society
Published on Web 06/03/2004

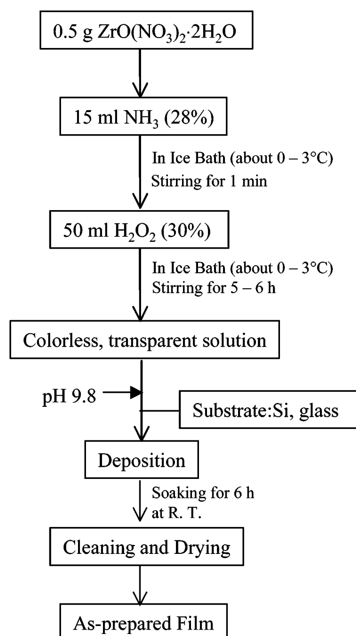

Figure 1. Schematic flowchart for the solution preparation and film deposition.

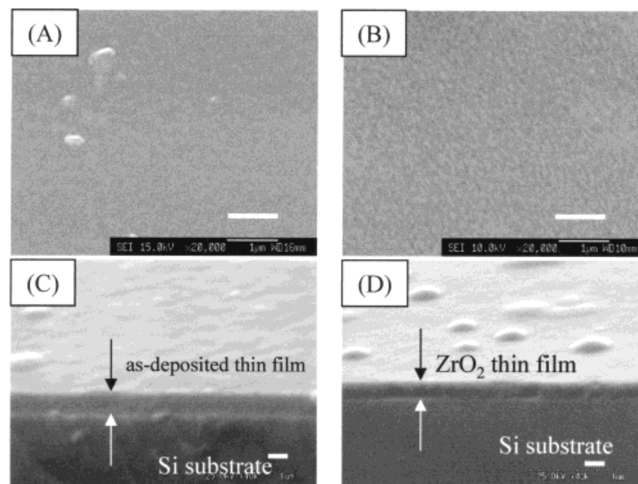

Figure 2. SEM photographs for the as-deposited thin film (A, C) and after annealing at 500 °C for 30 min in air (B, D). For cross-sectional observation, the samples were tilted at 75°. Scale bars are 1 μm for (A) and (B) and 200 nm for (C) and (D).

preparation conditions and use of an aqueous medium. However, it is difficult to eliminate the residual fluorine in the as-prepared thin film even by annealing, which restricts application of the film. From the viewpoint of "green" chemistry, it is preferable to prepare ZrO_2 thin film using an aqueous solution free of chlorine, fluorine, or sulfur.

In the present study, a method for preparing peroxozirconium-complex aqueous solution using simple inorganic substances such as $ZrO(NO_3)_2{\cdot}2H_2O$, $NH_3{\cdot}H_2O$, and H_2O_2 was established. By using this solution, a transparent, highly pure, amorphous ZrO_2-precursor thin film was synthesized on a Si wafer surface at room temperature. A tetragonal phase can be obtained after annealing at 500 °C for 30 min in air.

Experimental Section

Preparation of Precursor Solution and Deposition of Thin Films. The experimental flowchart is shown in Figure 1. Zirconium oxynitrate ($ZrO(NO_3)_2{\cdot}2H_2O$, 99.0%, Kishida), was selected as the Zr source. A mixture of hydrogen peroxide (H_2O_2, 30%, Kishida) and ammonia ($NH_3{\cdot}H_2O$, 28%, Kishida) in appropriate quantities was used as the solvent. Specifically, 0.5 g of $ZrO(NO_3)_2{\cdot}2H_2O$ was added to 15 cm^3 of ice-cooled ammonia and stirred for 1 min, then 50 cm^3 H_2O_2 was added. After the mixture was stirred for 4−5 h, the zirconium oxynitrate completely dissolved, and a homogeneous colorless and transparent solution was obtained. An ice bath was used to cool the solution for the entire time of solution preparation in the present research. The as-prepared peroxozirconium solution can maintain transparency for at least one week at temperatures near 0 °C, whereas it is unstable and became turbid after being stored at room temperature for longer than 1.5−2 h.

The substrate of 1.5 × 1.5 cm^2 Si wafer (P-type Si (100) wafer; Shinetsu) or barium borosilicate glass (Corning 1737) (for optical transmittance measurement only) was cleaned ultrasonically in acetone, ethanol, and deionized water (>18 MΩcm). After the substrate was dried at 50 °C, it was further irradiated by UV light (14.5 mW/cm^2) for 5 min. The cleaned substrate was then floated on the surface of the produced solution at room temperature (~20 °C) to deposit a thin film. After soaking for 6 h, the substrate was carefully rinsed with deionized water before vacuum-drying at 50 °C for 24 h.

Characterization. Phases, chemical composition, and morphology of the as-deposited thin film were characterized by X-ray diffraction (XRD; RAD-C, Rigaku; Cu Kα, 40 kV, 30 mA), X-ray photoelectron spectroscopy (XPS; ESCALAB 210, VG Scientific Ltd.; Mg Kα, 13 kV, 18 mA), and atomic force microscopy (AFM; SPI3800N, Seiko Instruments Inc.; scanning frequency 1−2 Hz), along with a scanning electron microscope (SEM; model S-3000, Hitachi). The thickness of the film was measured by a laser ellipsometer (PZ2000, Philips) with an incidence angle of 70° and wavelength of 632.8 nm. Optical transmission spectra were measured with a V-570 spectrophotometer (JASCO, resolution 100 nm·min^{-1}) at room temperature in a wavelength range of 200−1000 nm. Fourier transform infrared spectroscopy (FT/IR-610, JASCO) was performed at a resolution of 4 cm^{-1} with KBr as a reference. Thermogravimetric analysis (TG) and differential thermal analysis (DTA) (Thermo Plus TG8120, Rigaku, 5 °C/min) were conducted to further characterize the collected precipitate which was formed simultaneously with deposition of the thin film.

Results and Discussion

Film Morphology. The as-deposited thin film adhered well to the substrate as no peel-off was observed after either sonication (150 W) for 5 min in water or conducting the Scotch-tape peel-off test. Both the as-deposited thin film and that after annealing exhibited mirrorlike surfaces, implying smoothness of the surface and high packing density. The surfaces before and after annealing at 500 °C were flat as shown in the low-magnification SEM photographs (Figure 2A and B). Cross-sectional observation suggested that the film thickness, 200 nm for the as-deposited film (Figure 2C), decreased to less than 150 nm after annealing (Figure 2D), representing a shrinkage of more than 25% along the direction perpendicular to the substrate. This shrinkage is typically a result of film densification, bond reorganization, and/or the release of unstable components such as H_2O, hydroxyl groups, and carbonate, which were detected by FT-IR (see later part of this paper).

The AFM image (Figure 3A) clearly shows the particulate characteristics of the as-deposited thin film;

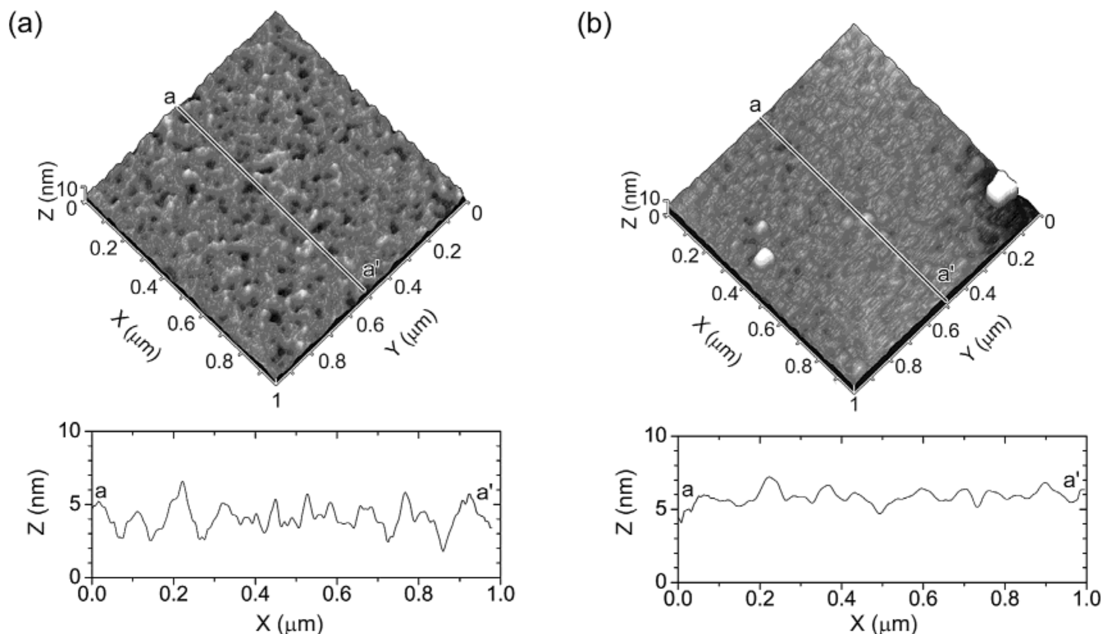

Figure 3. AFM images for the as-deposited thin film (a) and after annealing at 500 °C for 30 min in air (b). The bottom graphs of (a) and (b) show roughness profiles along the corresponding lines in (a) and (b), respectively.

particles with a mean diameter of about 40−50 nm can be observed on the surface. The particle size distribution is rather small, whereas dark-colored areas are still distributed among particles, indicating the presence of pores of nanometer size. The root-mean-square (RMS), representing surface roughness, is about 0.9−1 nm for the measured areas of 1 × 1 μm^2. This roughness is typical and easy to reproduce for the whole specimen with an area of 1 × 2 cm^2. The RMS value is of the same order as that for the substrate employed (about 0.4 nm), representing 0.5−1% of the film thickness. The AFM result is consistent with the SEM observation (Figure 2), which also revealed the formation of a very flat surface.

After the film was annealed at 500 °C, the particles became larger compared to those in the as-deposited thin film, while the diameter was still less than 60 nm (Figure 3B). The particles seemed to coalesce as the film shrank, contributing to an increase in particle size. Pores, which were present in the as-deposited film, were almost not observed in the annealed film, suggesting that the film became dense. However, the RMS roughness, 0.6 nm for the measured area of 1 × 1 μm^2, is still of the same order as that for the as-deposited film. It should be noted that no cracks appeared to be present according to SEM observation (Figure 2). Furthermore, no cracks were observed for the film less than 200 nm thick after annealing. At greater than this thickness, cracks were observed because of residual stresses.

XRD Results. Figure 4 shows the XRD profiles for the as-deposited thin film and those after annealing at different temperatures for 30 min in air. The as-deposited film was amorphous, as no obvious diffraction peaks were detected. Diffraction peaks appearing at about 30.1, 34.2, 35.1, 50.1, and 58.3° after annealing at 500 °C correspond to those from (101), (002), (110), (200), and (103) planes of tetragonal ZrO_2 (t-ZrO_2), respectively, suggesting crystallization into t-ZrO_2.

After the film was annealed at 600 °C, the appearance of a new phase, monoclinic-ZrO_2 (m-ZrO_2), was con-

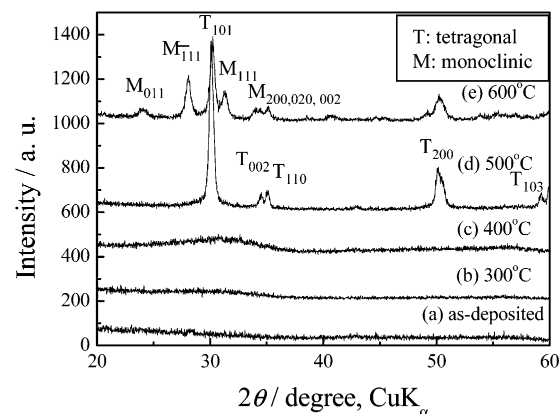

Figure 4. XRD profiles for (a) the as-deposited thin film and the films after annealing at different temperatures for 30 min in air: (b) 300 °C, (c) 400 °C, (d) 500 °C, and (e) 600 °C. The JCPDS file numbers for tetragonal and monoclinic phases are 42-1164 and 37-1484, respectively.

firmed, accompanying the decrease in intensity of (101) diffraction of t-ZrO_2. The coexistence of monoclinic and tetragonal ZrO_2 suggests that phase transformation occurred at 500−600 °C. This phase transformation has also been observed in ZrO_2 films grown through other chemical solution routes.[10−13,18]

The formation of metastable t-ZrO_2 phase, in preference to the thermodynamically preferred monoclinic polymorph at such low temperatures, has been attributed to the lower surface energy of the tetragonal phase compared to the monoclinic phase,[19] structural similarity between tetragonal and amorphous ZrO_2,[20−22]

(18) (a) Zhitomirsky, I.; Gal-Or, L.; Kohn, A.; Hennicke, H. W. *J. Mater. Sci.* **1995**, *30*, 5307. (b) Chaim, R.; Silberman, I.; Gal-Or, L. *J. Electrochem. Soc.* **1991**, *138*, 1943. (c) Chaim, R.; Stark, G.; Gal-Or, L.; Bestgen, H. *J. Mater. Sci.* **1994**, *29*, 6241.
(19) Garvie, R. C. *J. Phys. Chem.* **1978**, *82*, 218−224.
(20) Hu, M. Z.-C.; Hunt, R. D.; Payzant, E. A.; Hubbard, C. R. *J. Am. Ceram. Soc.* **1999**, *82*, 2313−2320 and references therein.
(21) Heuer, A. H.; Rühle, M. *Acta Metall.* **1985**, *33*, 2101.
(22) Garvie, R. C. *J. Phys. Chem.* **1965**, *69*, 1238.

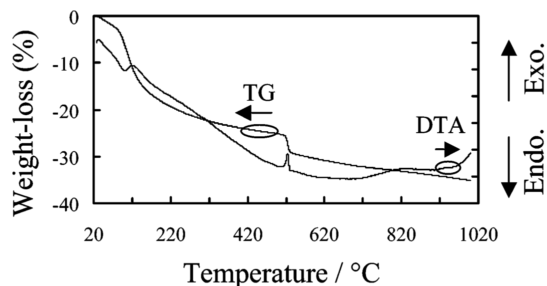

Figure 5. TG–DTA curves of the as-prepared precipitate.

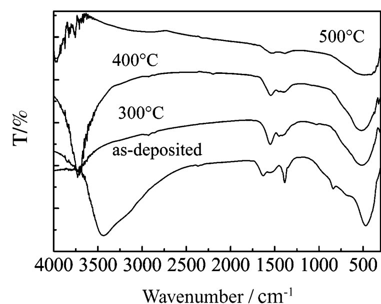

Figure 6. FT-IR spectra for the as-prepared powder and those after annealing at different temperatures.

or the presence of anionic impurities.[23] However, the surface energy theory cannot explain why monoclinic phase evolution occurred with increasing temperature rather than tetragonal phase growth. Anionic impurities such as OH^- have effects on the crystalline conversion. We have found residual hydroxyl groups in the films even after annealing at 400 °C (see XPS analysis in the latter part of this paper). The formation of zirconium hydroxide in solid form may be a major factor in the generation of t-ZrO_2 rather than m-ZrO_2 at low temperatures.

TG-DTA and FT-IR Analysis. Total weight loss (Figure 5) is 35%. Weight loss at $T < 150$ °C is 15% and attributed to adsorbed water. The 5% weight loss at 520–530 °C is associated with loss of residual OH and carbonate from film (see FT-IR analysis). The exothermic effect observed here might be attributed to the tetragonal–monoclinic phase transformation, consistent with the XRD result. Weight loss at above 530 °C is assigned to equipment errors. Exothermic reactions at 820 and 1000 °C were observed without weight loss and may be attributed to phase changes.

A FT-IR spectrum (Figure 6a) of the precipitate simultaneously collected during deposition of a thin film clearly showed the absorption bands assigned to the OH stretching at about 3442 cm^{-1}, water hydration at about 1627 cm^{-1}, and Zr–O at about 468 and 682 cm^{-1}.[10] A small band located at about 838 cm^{-1} in the as-prepared precipitate corresponds to a characteristic stretching of peroxo groups,[24] which disappeared after heating at 300 °C (Figure 6b). Bands at about 1380 and 1548 cm^{-1} were assigned to the vibration due to carbonate,[25] which were also detected for the as-deposited film by XPS (see the next section). The band located at 1627 cm^{-1} disappeared completely after annealing at 300 °C (Figure 6b), whereas peaks derived from CO_3^{2-} still existed even after annealing at 400 °C (Figure 6c) or 500 °C (Figure 6d). Hence, the complete elimination of CO_3^{2-} should have occurred at above 500 °C, which may have resulted in the abrupt weight loss at about 527 °C. The decomposition of CO_3^{2-} should be an endothermic reaction, whereas it did not appear in the DTA curve. It is assumed that this effect is very weak. After annealing at 500 °C, except those for CO_3^{2-}, appeared only bands assigned to t-ZrO_2.[10, 11, 26]

XPS Spectra. Chemical compositions of the as-deposited amorphous ZrO_2 thin film and those after annealing at different temperatures were further characterized by XPS. For the as-deposited thin film, XPS results suggest that only O, Zr, and a minor amount of C were present. The C_{1s} peak appearing near 284.6 eV in the spectrum was attributed to contamination, which is usually present as an impurity in the films prepared by either chemical or physical methods. Although no organic or carbon-containing raw materials were employed, a band located at about 295.0 eV was also detected which may be assigned to CO_3^{2-}.[27] This band was also detected for the film after annealing at 400 and 500 °C, although its intensity became significantly low, suggesting the presence of a trace of carbonate residue. Peaks for other impurities such as N and Si (attributed to the substrate) were not detected.

High-resolution scanning showed that the Zr_{3d} range for the as-deposited film was composed of two peaks with the binding energy of 182.6 ($Zr_{3d5/2}$) and 185.0 eV ($Zr_{3d3/2}$) (Figure 7a). The detected binding energy for $Zr3d_{5/2}$ is higher than those reported for Zr metal (180.0 eV) and ZrO_x ($0 < x < 2$, 181.4 eV), but close to 182.9 eV for ZrO_2.[28] After annealing at 400 and 500 °C (Figure 7b and c), the binding energies for $Zr_{3d5/2}$ were 182.6 and 182.7 eV, respectively. The corresponding values for $Zr_{3d3/2}$ were 185.0 and 185.1 eV, respectively.

The O_{1s} peak can be fitted to two peaks located at 529.8 and 531.6 eV with a molar ratio of about 1:1 for the as-deposited film (Figure 8a). The former is a characteristic value for ZrO_2, whereas the latter might have come from adsorbed water or OH groups,[28] the existence of which was also confirmed by FT-IR analysis. However, no peaks for peroxo groups were observed, which has a slightly higher binding energy (532–533 eV[29]), and was indeed detected for the as-deposited TiO_2 thin film prepared by the peroxotitanate-complex deposition method.[30,31] This finding suggests that the peroxozirconium complex was unstable compared to the

(23) Jolivet, J.-P.; Henry, M.; Livage, J. *Metal Oxide Chemistry and Synthesis*; John Wiley & Sons: Chichester, U.K., 2000.
(24) Gao, Y.-F.; Masuda, Y.; Peng, Z.-F.; Yonezawa, T.; Koumoto, K. *J. Mater. Chem.* **2003**, *13,* 608.
(25) (a) Arya, P.; Jha, P.; Ganguli, A. K. *J. Mater. Chem.* **2003**, *13*, 415–423. (b) Duran, P.; Capel, F.; Gutierrez, D.; Tartaj, J.; Banares, M. A.; Moure, C. *J. Mater. Chem.* **2001**, *11*, 1828–1836. (c) Gijp, S.; Winnubst, L.; Verweij, H. *J. Mater. Chem.* **1998**, *8*, 1251–1254.
(26) Phillipi, C. M.; Mazdiyasni, K. S. *J. Am. Ceram. Soc.* **1971**, *54*, 254.
(27) (a) Kumar, S.; Raju, V. S.; Kutty, T. R. N. *Appl. Surf. Sci.* **2003**, *206*, 250–261. (b) Ayouchi, R.; Martin, F.; Ramos-Barrado, J. R.; Leinen, D. *Surf. Interface Anal.* **2000**, *30*, 565–569. (c) Christie, A. B.; Lee, J.; Sutherland, I.; Wall, I. M. *Appl. Surf. Sci.* **1983**, *15*, 224.
(28) (a) Wang, Y. M.; Li, Y. S.; Wong, P. C.; Mitchell, K. A. R. *Appl. Surf. Sci.* **1993**, *72*, 237–240. (b) Brenier, R.; Mugnier, J.; Mirica, E. *Appl. Surf. Sci.* **1999**, *143*, 85.
(29) Rao, C. N. R.; Ganguly, P.; Hegde, M. S.; Sarma, D. D. *J. Am. Chem. Soc.* **1987**, *109*, 6893.
(30) Gao, Y.-F.; Masuda, Y.; Koumoto, K. *Langmuir* **2004**, *20*, 3188–3194.
(31) Gao, Y.-F.; Masuda, Y.; Koumoto, K. *Chem. Mater.* **2004**, *16*, 1062–1067.

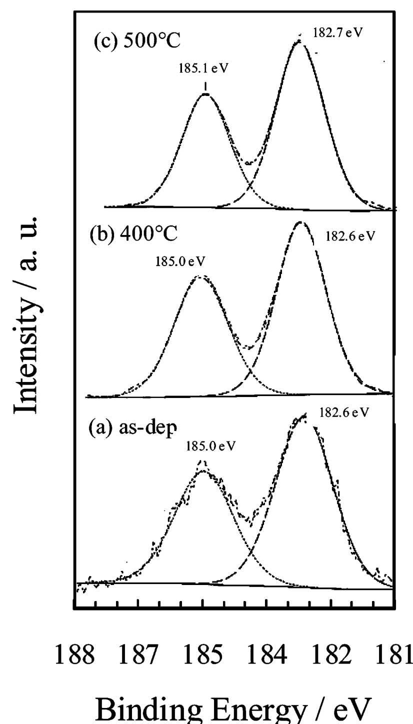

Figure 7. XPS spectra of the Zr_{3d} range for the as-deposited film (a) and those after annealing at 400 °C (b) and 500 °C (c).

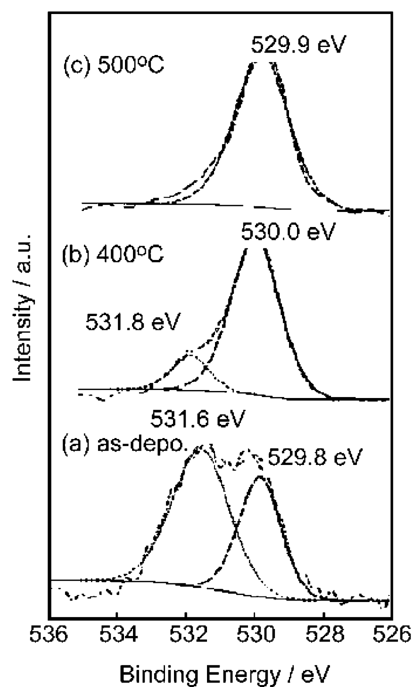

Figure 8. XPS spectra of the O_{1s} range for the as-deposited film (a) and those after annealing at 400 °C (b) and 500 °C (c).

peroxotitanate complex. The peak attributed to the hydroxyl group weakened significantly after annealing at 400 °C (Figure 8b), and finally disappeared after annealing at 500 °C (Figure 8c).

The quantitative analysis (by area) shows a molar ratio of Zr/O = 1:2.55 for the as-deposited thin film, which is much smaller than the value for stoichiometric ZrO_2, suggesting that oxygen is partially in the OH or H_2O state. However, a ZrO_2 thin film with the stoichiometric composition of Zr/O = 1:2 was obtained after annealing at 400 or 500 °C, but the small peak for Zr−OH in the Zr_{3d} range confirmed that the elimination of impurities (mostly in the form of H_2O or OH) was not complete even after annealing at 400 °C. On the basis of XRD, FT-IR, TG-DTA, and XPS results, we propose that the chemical formula for the as-deposited thin film should be $ZrO_{1.4}(OH)_{1.2}$, which represents a theoretical weight loss of about 9%.

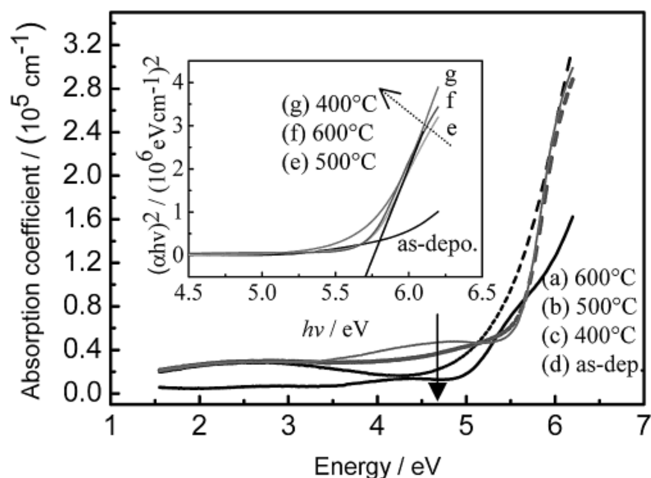

Figure 9. Absorption spectra of the as-deposited thin film and those after annealing at different temperatures. Inset shows direct band gaps of the as-deposited thin film and those after annealing at different temperatures.

Transparency and Optical Band Gap. For the determination of optical band gap, the ZrO_2 thin film was prepared on a glass substrate under the same conditions as those prepared on Si substrates. All the amorphous and crystallized ZrO_2 thin films showed little absorption in the visible region, implying high transparency (Figure 9). In fact, the mean transmittance in the visible region was over 85% and 65% for the as-deposited thin film and those after annealing, respectively, on the basis of transmittance spectra. The high transparency indicates fairly smooth surfaces and relatively good film homogeneity, which is consistent with the AFM observations. The decrease in transmittance suggests that the cracks appeared in the film after annealing. Obvious absorption-edge shifts were not obtained for our films, but there were differences in the rate of change of absorption coefficient near the absorption edge for films heated at different temperatures. These differences are ascribed to the containment of defects in the as-deposited film or the quantum confinement effects. Slight coloration of ZrO_2 after annealing was observed by the naked eye. XPS analysis showed that the film was pure except for a trace of carbonate, so that the coloration was not due to the presence of impurities, but can be attributed to defects.

For the high-energy absorption region, the relation between transmittance (T) and absorption coefficient (α) can be expressed as: $\alpha = -\ln(T)/d$, where d is the film thickness.[24] The film thickness was measured by laser ellipsometer to be 205, 160, 158, and 158 nm for the as-deposited thin film and those after annealing at 400, 500, and 600 °C, respectively. The direct band gap, E_g, can be estimated from analyzing the spectra in the region where a steep increase of the adsorption was observed. In this region, band-to-band transition is characteristic and the band gap can be determined by using the formula $(\alpha h\nu) = A(h\nu - E_g)^{1/2}$, where $h\nu$ is

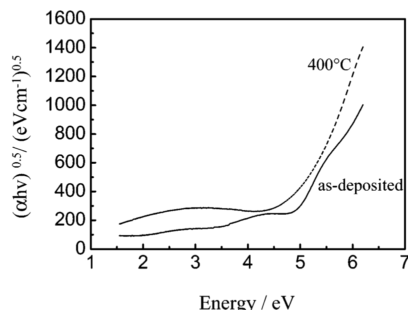

Figure 10. Tauc gaps for the as-deposited film and that after annealing at 400 °C.

incident photon energy and A is a constant.[24]

The inset of Figure 9 shows the $(\alpha h\nu)^2$ versus $h\nu$ curve for the as-deposited thin film and those annealed at different temperatures. Band gap energies were evaluated by extrapolating the linear parts of the curves to the energy axis. For the crystal films annealed at 500 or 600 °C, the relation was highly linear, giving band gaps with almost the same value of 5.65 eV, which is slightly higher than those for amorphous films. However, the Tauc band gap for the amorphous film, whether annealed (at 400 °C) or not, was about 4.5–4.6 eV (Figure 10). The difference is associated with structural disorder and defects in the amorphous state.[32]

There are three points worth noting concerning the derived band gap energies. First, the values obtained in this study are comparable with most of the reported ones (5.78 eV for t-ZrO_2 and 5.83 eV for m-ZrO_2 (bulk),[33] 5.87 eV (bulk t-ZrO_2),[34] 5.42 eV (m-ZrO_2),[35] 4.88–5.44 eV (doped thin film),[36] 5.62 eV (doped thin film),[37] 5.85 eV (powder),[38] 5.6 eV (thin film)[39]). However, they are much higher than that for ZrO_2 thin film prepared by sputtering (4.52–4.67 eV[39]).

Second, the band gap energy for the amorphous film, especially the as-deposited one, is significantly different from those for the crystallized films. Similar phenomena were also observed in our previous studies,[24,40] and have attributed to the structural disorder and defects in the amorphous film.[32] It is known that in a defect-free crystalline semiconductor the absorption spectrum terminates abruptly at the wavelength corresponding to the energy gap, below which no absorption is observed. Hence, one can define the absorption edge of a crystalline semiconductor experimentally. In contrast, in an amorphous semiconductor, a tail in the absorption spectrum encroaches into the gap region. This tail state is usually localized by the site disorder, and a critical energy, called the mobility edge, separates the localized state from the extended state. The existence of a tail state makes it difficult to define the absorption edge experimentally and leads to large errors when calculating the band gap energy of an amorphous thin film. This may be responsible for the unexpected lower band gap for the amorphous film.

Third, the quantum confinement effect is not obvious for our film annealed at 500 and 600 °C, probably because the grain sizes are beyond some critical value. The band gap energy changes very significantly when the grain size decreases below 30 nm,[37] whereas we observed grain sizes of about 50–60 nm for our annealed films.

Aqua Chemistry of Zirconium and Solid-Phase Deposition Mechanism. Among the Group 4 elements, Ti(IV) can form monomeric $[Ti(OH)_2]^{2+}$ ("TiO^{2+}") (aq) species according to calculations based on the partial charge model.[23,41] However, Zr(IV) has a higher coordination number (8) than that of Ti(IV) (6). As a result, the precursor monomers $[Zr(OH)(OH_2)_7]^{3+}$ and $[Zr(OH)_2(OH_2)_6]^{2+}$ are much less acidic than $[Ti(OH)(OH_2)_5]^{3+}$, implying that OH groups in Zr(IV) aqua monomers present a negative partial charge. This tends to promote condensation to form the OH-bridged tetramers. Experimental studies have also suggested that hydrolytic polymerization occurs extensively even in acidic conditions to produce OH-bridged polynuclear chains and/or clusters.[42] It is clear now that a tetramer of $[Zr_4(OH)_8(OH_2)_{16}]^{8+}$ is probably present in the aqueous solutions of Zr(IV) salts.[23] In this aqua ion, two adjacent zirconium atoms are doubly bridged by two hydroxyl ligands. In an acidic aqueous solution containing H_2O_2, a tetranuclear peroxozirconium-complex ion having the formula $[Zr_4(O_2)_2(OH)_4(OH_2)_{16}]^{8+}$ (aq) was also reported.[43] Although not precisely, it seems that the structure is constructed by two peroxide ions replacing four bridging hydroxide ions in $[Zr_4(OH)_8(OH_2)_{16}]^{8+}$. However, no studies discussed whether such an aqua ion can exist under highly basic conditions. Our studies experimentally confirmed the possibility of formation of the peroxozirconium complex even under strongly basic conditions (pH = ~9.8).

For deposition of ZrO_2 thin film from a solution, it is necessary to predict the reactivity of Zr(IV) during hydrolysis, condensation, or complexation. Understanding the chemistry of zirconium is also desirable for tuning film properties such as thickness, growth rate, chemical composition, and crystallite size. Jolivet and co-workers have developed a partial charge model as a guide for understanding these issues.[23] They state that

(32) Thomas, P.; Overhof, H. Amorphous Semiconductors: Localization. In *The Encyclopedia of Materials: Science and Technology*; Elsevier Science Ltd.: New York, 2001; pp 277–283.
(33) French, R. H.; Glass, S. J.; Ohuchi, F. S.; Xu, Y.-N.; Ching, W. Y. *Phys. Rev. B* **1994**, *49*, 5133.
(34) Aita, C. R.; Hoppe, E. E.; Sorbello, R. S. *Appl. Phys. Lett.* **2003**, *82*, 677.
(35) Kralik, B.; Chang, E. K.; Louie, S. G. *Phys. Rev. B* **1998**, *57*, 7027.
(36) Zhang, Y.-W.; Jin, S.; Liao, C.-S.; Yan, C.-H. *Mater. Lett.* **2002**, *56*, 1030.
(37) Kosacki, I.; Petrovsky, V.; Anderson, H. U. *Appl. Phys. Lett.* **1999**, *74*, 341.
(38) Emeline, A.; Kataeva, G. V.; Litke, A. S.; Rudakova, A. V.; Ryabchuk, V. K.; Serpone, N. *Langmuir* **1998**, *14*, 5011.
(39) Hartridge, A.; Krishna, M. G.; Bhattacharya, A. K. *Thin Solid Films* **2001**, *384,* 254.
(40) Gao, Y.-F.; Masuda, Y.; Koumoto, K. *J. Kor. Ceram. Soc.* **2003**, *40*, 213.
(41) (a) Beukenkamp, F. L.; Herrington, K. D. *J. Am. Chem. Soc.* **1960**, *82*, 3025. (b) Caglioti, V.; Ciavatta, L.; Liberti, A. *J. Inorg. Nucl. Chem.* **1960**, *15*, 115. (c) Rotzinger, F. P.; Grätzel, M. *Inorg. Chem.* **1987**, *26*, 3704. (d) Tompson, G. A. K.; Taylor, R. S.; Sykes, A. G. *Inorg. Chem.* **1977**, *16*, 2880.
(42) Zielen, A. J.; Connick, R. E. *J. Am. Chem. Soc.* **1956**, *78*, 5785.
(43) Thompson, R. C. *Inorg. Chem.* **1985**, *24*, 3542.
(44) Ficher, A.; Jentoft, F. C.; Weinberg, G.; Schögl, R.; Niesen, T. P.; Bill, J.; Aldinger, F.; De Guire, M. R.; Rühle, M. *J. Mater. Chem.* **1999**, *14*, 3725.
(45) Aiken, B.; Hsu, W. P.; Matijevic, E. *J. Mater. Sci.* **1990**, *25*, 1886.
(46) Gao, Y.-F.; Masuda, Y.; Yonezawa, T.; Koumoto, K. *Chem. Mater.* **2002**, *14*, 5006–5014.
(47) Cölfen, H.; Schnablegger, H.; Fischer, A.; Jentoft, F. C.; Weinberg, G.; Schlögl, R. *Langmuir* **2002**, *18*, 3500–3509.
(48) Gao, Y.-F.; Koumoto, K. unpublished results.

when two atoms combine, partial electron transfer occurs so that each atom acquires a positive or negative partial charge, which results in the increase or decrease in the electronegativities of related atoms. The electron transfer continues until the electronegativities of all the constituent atoms become equal to the mean electronegativity.[23] According to this model, the calculated partial charge for the water molecules ($\delta(H_2O)$) is closely related to the tendency of the metal ions to form either an oxide precipitate or a mixed hydroxide/oxyhydroxide precipitate. For the aqua ion of zirconium $\delta(H_2O)$ is positive, so the water molecule is repelled by the metal center, allowing the formation of the oxo bridge. Hence, zirconium will hydrolyze and condense to generate zirconium oxide or oxyhydroxide depending on the solution conditions.

Generally, zirconium (IV) cations have a strong tendency to hydrolyze in aqueous media, and solutions typically turn cloudy and a precipitate is formed. The impurities appearing in the precipitate are closely related to complexes formed in solution. The electronegativity–pH diagram[23] for the aqua ion of $[Zr_4(OH)_8(OH_2)_{16}]^{8+}$ suggests that Cl^- is retained in the solid of zirconia when it is precipitated at higher pH. The sulfate ion (SO_4^{2-}) is easier to complex with zirconium than Cl^- and can form various complexes of zirconium over a wide range of pH. Significant amounts of impurities such as Cl^- or SO_4^{2-} should be easily embedded in the ZrO_2 when prepared under these conditions, which has been proved experimentally.[10,42,44] At higher pH, the sulfate group, weakly coordinated to the metal ion, is easily replaced by other anions.[10] In an aqueous solution containing zirconium sulfate and urea, a basic zirconium carbonate ($Zr_2(OH)_6CO_3{\cdot}2H_2O$) may be precipitated.[45] F^- also has a strong ability to form complexes in the solution with many metal ions such as Si(IV), Ti(IV), and Zr(IV), therefore precipitation of F into the corresponding oxides is well-known in the LPD method.[15–17,46] Conversely, the nitrate ion in the zirconium solution is neither strongly complexing nor bridging, and does not form complexes with zirconium except in concentrated nitric acid.[23,47] Therefore, we can obtain ZrO_2 thin films free of nitrogen, which was confirmed by XPS analysis. It is also convenient for us to deal with Zr(IV) as the tetramer polycation as in the case of the $ZrOCl_2{\cdot}8H_2O$ when $ZrO(NO_3)_2{\cdot}2H_2O$ is used as the raw material.

On the basis of the above discussion, we propose the following formation mechanism for precipitation of ZrO_2 in the peroxozirconium complex solution. First, a ligand exchange reaction occurred between $ZrO(NO_3)_2$ and NH_4OH to produce an intermediate solid of $ZrO(OH)_2$ (eq 1), which dissolved to present the corresponding aqua ion. Second, the aqua ion reacted with H_2O_2 and NH_4OH, forming a peroxozirconium complex, the tetramer $[Zr_4(O_2)_2(OH)_4(OH_2)_{16}]^{8+}$ (eq 2).[43] A structure determination for this peroxo complex was not experimentally conducted in the present research partially because the preparation of corresponding single crystals was not successful. Formally, peroxide ions replace four bridging hydroxide ions. After this reaction had completed, the solution became transparent and colorless. Third, when the solution temperature was increased, peroxo groups in the peroxozirconium complex decomposed by the release of O_2. As a consequence, the partial charge of the OH group in the $[Zr_4(O_2)_{2-x}(OH)_4(OH_2)_{16}]^{8+2x}$ became more negative. Condensation was therefore promoted, producing zirconium oxyhydroxide ($ZrO_{1.4}(OH)_{1.2}$, eq 3). In the present reaction for producing ZrO_2 oxide, hydroxyl groups were needed to improve the condensation, which was confirmed by accurate measurement of the solution pH. Typically, the pH of the as-prepared transparent solution was about 9.8, which decreased to about 9.2 when the solution recovered to be transparent after reaction for 48 h. When the initial pH was reduced, the solution tended to be stable rather than unstable, implying that the formation of solid is postponed. In contrast, the formation of TiO_2 in the peroxotitanium complex solution requires absorption of protons; hence, lowering the pH (in a specific range) has effects on accelerating the precipitation of oxide.[48] Fourth, ZrO_2 was obtained after dehydration and release of hydroxyl groups by annealing (eq 4). The weight loss due to the as-deposited ZrO_2 precursor was not observed above 400 °C, which is lower than the crystallization temperature (500 °C), suggesting the formation of an amorphous ZrO_2. Last, the structure rearrangement based on thermodynamics promotes the polymorphic transformation (eq 5).

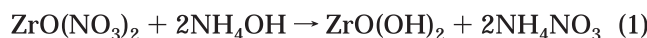

$$ZrO(NO_3)_2 + 2NH_4OH \rightarrow ZrO(OH)_2 + 2NH_4NO_3 \quad (1)$$

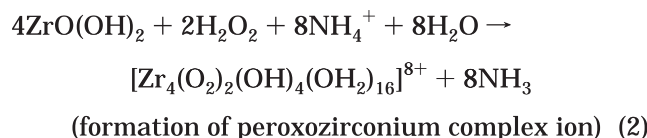

$$4ZrO(OH)_2 + 2H_2O_2 + 8NH_4^+ + 8H_2O \rightarrow [Zr_4(O_2)_2(OH)_4(OH_2)_{16}]^{8+} + 8NH_3$$

(formation of peroxozirconium complex ion) (2)

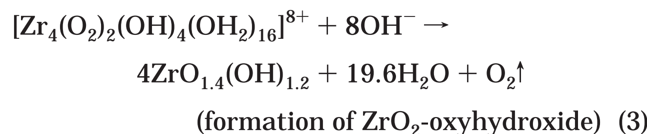

$$[Zr_4(O_2)_2(OH)_4(OH_2)_{16}]^{8+} + 8OH^- \rightarrow 4ZrO_{1.4}(OH)_{1.2} + 19.6H_2O + O_2\uparrow$$

(formation of ZrO_2-oxyhydroxide) (3)

$$ZrO_{1.4}(OH)_{1.2} \rightarrow ZrO_2\ (\text{amorphous}) + 0.6H_2O \quad (4)$$

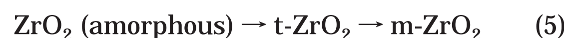

$$ZrO_2\ (\text{amorphous}) \rightarrow \text{t-}ZrO_2 \rightarrow \text{m-}ZrO_2 \quad (5)$$

Conclusions

Amorphous, homogeneous, flat ZrO_2 thin films of tens to 500 nm thick were prepared on a P-type Si or glass substrate. The film showed good adhesion to the substrate as the deposits could not be peeled off by either sonication or a Scotch-tape peel-off test. The as-deposited thin film could transform to tetragonal and/or monoclinic ZrO_2 after annealing at different temperatures. The as-deposited film was composed of closely packed homogeneous nanoparticles of 40–50-nm diameter, and showed a very flat surface with a RMS roughness of 0.9–1 nm for a measured area of 1×1 μm^2. After annealing, the particle size increased slightly, but the flatness of the surface remained. The as-deposited thin film was of high purity with a formula of $ZrO_{1.4}(OH)_{1.2}$. Heating resulted in dehydration and release of hydroxyl groups and produced stoichiometric ZrO_2 thin film, either amorphous or crystalline. Both the as-deposited thin film and those after annealing were highly transparent. The optical band gap for the crystalline ZrO_2 thin films was 5.65 eV regardless of their phase structures, which is comparable with those

reported for bulk or film-form ZrO_2. The ZrO_2 deposition mechanism was also discussed.

Acknowledgment. Y.F.G. expresses his gratitude to the China Scholarship Council for providing a scholarship (State Scholarship for Excellent Chinese Students Studying Abroad). This work was supported in part by the 21st Century COE (Center of Excellence) Program "Nature-Guided Materials Processing" of the Ministry of Education, Culture, Sports, Science and Technology, Japan.

Note Added after ASAP Posting. The *x* and *y* axes of Figure 6 were incorrectly labeled in the version posted ASAP June 3, 2004; the final web version and print version are correct.

CM049771I